Gas-Aggregated Copper Nanoparticles with Long-term Plasmon Resonance Stability

Vladimir N. Popok[1] · Sergey M. Novikov[2] · Yurij Yu. Lebedinskij[3,4] · Andrey M. Markeev[4] · Aleksandr A. Andreev[5] · Igor N. Trunkin[5] · Aleksey V. Arsenin[2] · Valentyn S. Volkov[2]

Abstract

Metal nanoparticles (NPs) possessing localized surface plasmon resonance (LSPR) are of high interest for applications in optics, electronics, catalysis, and sensing. The practically important issue is the stability of the LSPR, which often limits the use of some metals due to their chemical reactivity leading to degradation of the NP functionality. In this work, copper NPs of two distinct sizes are produced by magnetron sputtering gas aggregation. This method ensures formation of the particles with high purity and monocrystallinity, enhancing the chemical inertness and providing a superior time stability of the plasmonic properties. Additionally, a simple UV-ozone treatment, which leads to the formation of an oxide shell around the copper NPs, is found to be an efficient method to prevent following gradual oxidation and assure the LSPR stability in ambient atmospheric conditions for periods over 100 days even for small (10–12 nm in diameter) NPs. The obtained results allow for significant improvement of the competitiveness of copper NPs with gold or silver nanostructures, which are traditionally used in plasmonics.

Keywords Gas aggregation nanoparticle formation · Copper nanoparticles · Copper oxidation · Localized surface plasmon resonance

Introduction

Metal nanoparticles (NPs) in a dielectric environment are well known for the phenomenon of localized surface plasmon resonance (LSPR) resulting in a strong enhancement of optical extinction and local electric field [1, 2]. This phenomenon is of great interest for applications in many areas, such as non-linear optics, electronics, photovoltaics, catalysis, and sensing [3–8]. Although many metals on the nanoscale show considerable plasmonic efficiency, only a few provide LSPR in the visible range of the spectrum. Among those, gold NPs are the most used ones due to their strong plasmonic resonance, high chemical stability, low toxicity, and good abilities of surface functionalization [9]. Silver nanostructures are also widely used but generally considered less attractive due to their requirements for blue-near UV light for plasmon excitation and lower chemical and, thus, plasmonic stability, which is often assigned to oxidation [10, 11]. Recent studies have shown that the degradation of silver plasmonic properties is also caused by reactions with sulfur, which even is present in trace amounts in ambient atmosphere [12, 13].

One more candidate with LSPR in the visible spectral range is copper. NPs of this metal can provide intense and narrow plasmonic bands at wavelengths between approximately 500 and 800 nm [1, 14]. It has been recently reported that copper can outperform gold in waveguide applications and it is compatible with complementary metal–oxide–semiconductor technologies [15, 16]. However, copper nanostructures are even less chemically stable than those of silver. Copper is prone to relatively fast surface oxidation upon exposure to ambient atmosphere. At room temperature, the dominant product is Cu_2O (Cu(I) oxide) with a minor or no contribution of CuO (Cu(II) oxide) [17]. In the in situ transmission electron

✉ Vladimir N. Popok
vp@mp.aau.dk

1 Department of Materials and Production, Aalborg University, 9220 Aalborg, Denmark

2 Center for Photonics and 2D Materials, Moscow Institute of Physics and Technology, Dolgoprudny, Russia 141700

3 Center of Shared Facilities in Nanotechnology, Moscow Institute of Physics and Technology, Dolgoprudny, Russia 141700

4 Institute of Laser and Plasma Technologies, National Research Nuclear University, Moscow, Russia 115409

5 National Research Center, «Kurchatov Institute», Moscow, Russia 123182

microscopy (TEM) studies on dynamic oxidation of Cu NPs, it was observed that the process can undergo via the oxide phase nucleation on one side of the NP with following progressing across the entire particle until full oxidation occurs [18]. For the use of copper NPs in plasmonic applications, a protection against oxidation-induced degradation of properties is required. It can be done by incorporating the NP into a substrate [19–21] or the formation of a shell/coating [22]. The latter is a common approach for the fabrication of commercial Cu NPs, but they are still prone to oxidation, not preserving the plasmonic behavior on a long time scale [23].

It is worth mentioning that the opinion about fast chemical degradation of silver and copper is mostly based on the studies of NPs prepared by wet chemical methods or by physical means involving a self-aggregation process or lithography. In these cases, the crystallinity of the nanostructures is often questionable; the presence of structural defects or contaminants is highly probable promoting the chemical reactions with ambient gases or volatile compounds. Alternatively, NPs with high chemical purity and perfect crystalline structure can be prepared in vacuum using a gas aggregation (cluster beam) method [24, 25]. In gas aggregation sources, atoms of metal NPs are densely packed following the highly symmetric polyhedral shapes according to Wulff construction [26–28]. In such monocrystalline polyhedral NPs, the facet atoms have higher coordination numbers compared with polycrystalline particles of arbitrary shape, thus, exhibiting a low chemical reactivity. The chemical inertness enhances stability of the plasmonic properties, as was shown for the case of silver NPs [29].

In the current work, systematic investigations of the plasmonic properties of gas-aggregated copper NPs produced by the magnetron sputtering method and stored in different environments are carried out. They are supported by a detailed study of structure and composition. The obtained results provide important practical insights on handling the NPs in order to ensure their long-time stability of the functional properties.

Experimental

Cu NP Fabrication and Treatment

Copper NPs were produced by the magnetron sputtering cluster apparatus, called MASCA. More details about the system and typical operation parameters can be found elsewhere [30, 31]. In the current experiments, a Cu target with 99.99% purity was used for the NP formation. Typical background pressure in the source chamber was $(4–6) \times 10^{-8}$ mbar, increased up to $(2–3) \times 10^{-3}$ mbar during magnetron operation. Background pressure in the deposition chamber was kept at $(2–3) \times 10^{-7}$ mbar (increased to $(5–6) \times 10^{-6}$ mbar during

deposition). The NPs were filtered using the electrostatic quadrupole mass selector [32] at voltages of 600 and 1200 V, thus, selecting NPs of two different sizes (diameters). The NPs were deposited in a soft-landing regime (with energies in meV/atom range) on quartz substrates for optical spectroscopy measurements, Si substrates for Auger/X-ray photoelectron spectroscopy (XPS), and carbon-coated grids for TEM.

Three sets of samples were made for every NP size. One set was always kept in ambient (laboratory) atmospheric conditions. The second one was placed into a hermetic box with continuous N_2 flow under pressure > 1 bar. These samples were taken to ambient atmosphere for a short time to perform the optical measurements: once a day during the first 5 days and once every 4–5 days after that. Samples of the third set were treated using a standard UV-ozone laboratory cleaner (Bioforce Nanosciences) for 20 min immediately after the deposition and then kept in ambient atmosphere. During this treatment, the UV light at 189.9 nm cracks molecular oxygen and the produced atomic oxygen can form ozone molecules. O_3 can be further decomposed by light with wavelength of 253.65 nm. All three sets of samples were stored at room temperature.

Cu NP Characterization

In order to find the size, structure, and composition of the prepared NPs, atomic force microscopy (AFM), TEM, and XPS measurements were carried out. AFM was performed directly after the depositions in tapping mode using an Ntegra Aura system (NT-MDT) and commercial ultra-sharp silicon cantilevers. The TEM and electron diffraction analysis was carried out by a Titan 80-300 TEM/STEM (Thermo Fisher Scientific) with a spherical aberration corrector in the bright- and dark-field modes. For the latter, the samples were scanned using a high-angle annular dark-field detector of scattered electrons. The accelerating voltage was 300 kV. High-resolution (HR) TEM images were recorded using a CCD camera (Gatan), 4×4 megapixel. Chemical state and composition of the Cu NPs were analyzed by XPS using the Theta Probe tool (Thermo Scientific) under high-vacuum conditions with a monochromatic Al Kα X-ray source (1486.6 eV). The TEM and XPS analyses were carried 2 weeks after the Cu NP deposition. These samples were kept in air between the deposition/treatment and measurements.

The extinction spectra are obtained from optical transmission measurements using a double beam PerkinElmer high-performance lambda 1050 spectrometer in standard configuration. A code is built in MatLab in order to simulate plasmonic properties of the NPs using Mie theory. In the model, we take into account only absorption cross-section C_{abs} because light scattering is low for metal NPs with small radii like in our case [1, 2]. The cross-section is calculated using following equation:

$$C_{abs} = 4\pi k r^3 \mathrm{Im} \frac{\epsilon_r + \epsilon_i - \epsilon_m}{\epsilon_r + \epsilon_i + 2\epsilon_m} \quad (1)$$

where k is the wave vector, r is the particle radius, and ε_r and ε_i are the real and imaginary dielectric functions of the metal (taken from [33]), respectively, while ε_m is the dielectric constant of the medium.

Results and Discussion

Structure and Composition of Cu NPs

The AFM measurements yielded typical heights of 10–13 and 18–20 nm for the filtering voltages of 600 and 1200 V, which are further referred to as small and large NPs, respectively. The obtained values show a good agreement with earlier calibration dependence of NP size vs. filtering voltage [30]. Soft-landed Cu NPs are known to preserve an almost spherical shape; they just slightly oblate having an aspect ratio (diameter-to-height) of 1.15 [32]. Thus, the height measurements provide a good estimate of the mean particle diameter.

TEM and HR TEM images with fast Fourier transform (FFT) of diffraction patterns for the Cu NPs are presented in Fig. 1. The obtained mean NP diameters of ca. 10 nm and ca. 18 nm for the small and large NPs, respectively, show good agreement with those found by AFM. The FFT patterns reveal the formation of monocrystalline metallic Cu NPs with *fcc* structure [34]. The results on *fcc* structure correlate well with earlier data obtained on the gas-aggregated Cu NPs [32]. In the diffraction images, one can also observe the presence of Cu_2O, which is known to be the dominant oxide forming in ambient atmosphere [17]. It is a result of oxidation after taking the particles out from vacuum.

During UV-ozone treatment, the mixture of atomic oxygen and ozone leads to an intensive oxidation of the Cu NPs. The TEM images reveal a shell formation around a metallic core

(see Fig. 2b). While for the particles oxidized in ambient atmosphere, Cu_2O dominates, for the UV-ozone-treated NPs, the oxidation undergoes mainly through the formation of CuO (see FFT patterns in Fig. 2a). The latter is in good agreement with data published elsewhere reporting a predominant formation of CuO by UV-ozone treatment of metallic Cu surfaces [35]. The oxidation issue is further addressed in the analysis of XPS data presented below.

Figure 3a shows Auger Cu LMM peaks of the NPs kept in ambient air indicating the dominant Cu_2O component with a weak shoulder of metallic Cu for the small particles and a bit stronger one for the large ones. The TEM images do not reveal any core/shell structures for these samples. Hence, one can suppose that the oxidation undergoes from one (for example, a top) side of the NP. Such way of oxidation was found earlier [18]. Since the depth of Auger analysis is low, ≤ 2 nm, the oxide layer thickness can be 1–2 nm because the signals from the metallic phase are weak but still seen. The studies published elsewhere [17] showed that a 1–2-nm-thick oxide shell growth requires 2–3 weeks, which correlates well with our results because the measurements were carried out 2 weeks after the deposition and the particles have been kept in air. The XPS spectra presented in Fig. 3b show the characteristic bands at 932.6 and 952.4 eV related to $Cu2p_{3/2}$ and $Cu2p_{1/2}$ states, respectively, as well as a satellite band at 945 eV. Cu and Cu_2O have nearly the same binding energy [36, 37]; thus, it is impossible to resolve the contributions of metallic Cu and Cu(I) oxide. However, the relatively broad $Cu2p_{3/2}$ band supports the domination of Cu_2O, which also correlates with the Auger data. The presence of shoulders at 933.6 and 954.5 eV provides evidence for a small contribution of CuO. Thus, the Auger and XPS results agree well with each other as well as with the diffraction data on the dominant Cu(I) oxide formation in ambient atmosphere.

Spectra of the NPs treated with UV-ozone are shown in Fig. 3c and d. The broadening of the Cu LMM band, which can be seen in Fig. 3c, compared with the case presented in Fig. 3a indicates a stronger contribution of CuO, while no clear

Fig. 1 **a** TEM and **b** HRTEM images for small Cu NPs. In panel (**b**), corresponding FFT diffraction patterns are presented
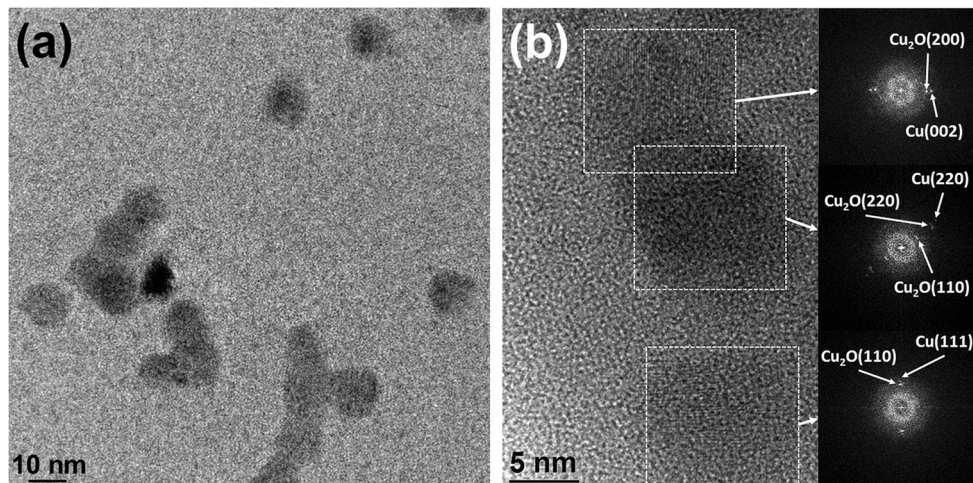
Fig. 2 **a** HRTEM image with FFT patterns for small Cu NPs treated with UV-ozone and **b** high-angular annular dark-field image for large Cu NP treated by UV-ozone
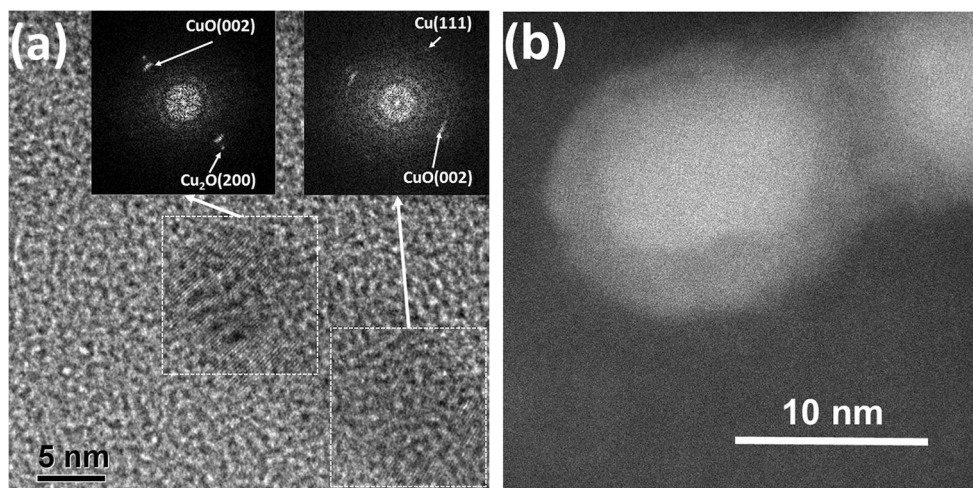
evidence for metallic Cu is present. Hence, the formed oxide shells should be thicker than the escape depth of electrons. Indeed, as one can see in Fig. 2b, the shell thickness reaches 3 nm. The XPS spectra presented in Fig. 3d show a significant increase of the $Cu2p_{3/2}$ and $Cu2p_{1/2}$ shoulders at 934.7 and 954.5 eV, respectively. The latter is known to be assigned to Cu(II) oxide, while the former can correspond to copper dihydroxide, $Cu(OH)_2$ [37]. Presence of $Cu(OH)_2$ was also reported elsewhere [35] for UV-ozone-treated Cu surfaces, thus,

demonstrating a good correlation of the results. In Fig. 3d, one can also observe two new strong satellite peaks of Cu^{2+} at 941 and 963 eV, which are typical for CuO [37]. Thus, the XPS and Auger data are in good agreement with those of TEM/diffraction for the ozonated samples. The obtained results show a significant difference in the NP oxidation under ambient conditions and UV-ozone treatment. Namely, in ambient atmosphere, the NPs predominantly form Cu(I) oxide, while under UV-ozone treatment, mainly Cu(II) oxide is grown.

Fig. 3 Auger spectra of Cu, CuO, and Cu_2O bands (kinetic energies are indicated by dashed and dotted lines) **a** before and **c** after UV-ozone treatment. XPS spectra of Cu2p states with fits of CuO and Cu_2O **b** before and **d** after UV-ozone treatment. The spectra for the samples with small and large copper NPs are indicated as "small" and "large," respectively
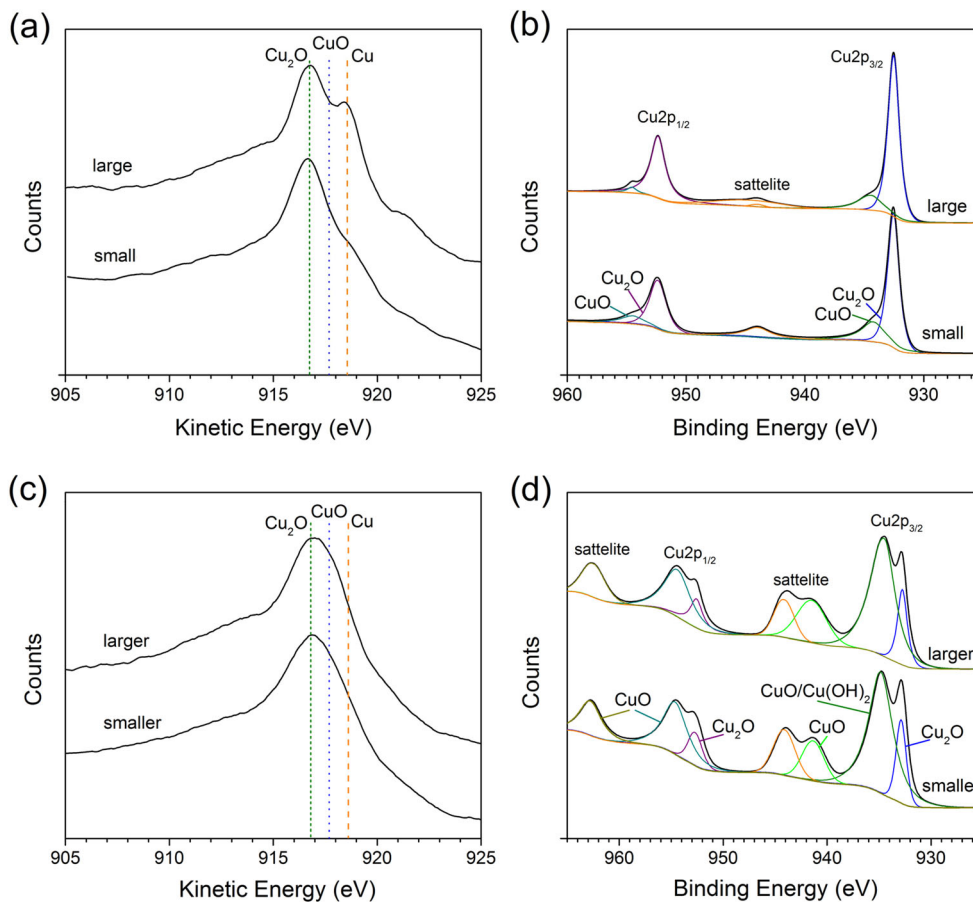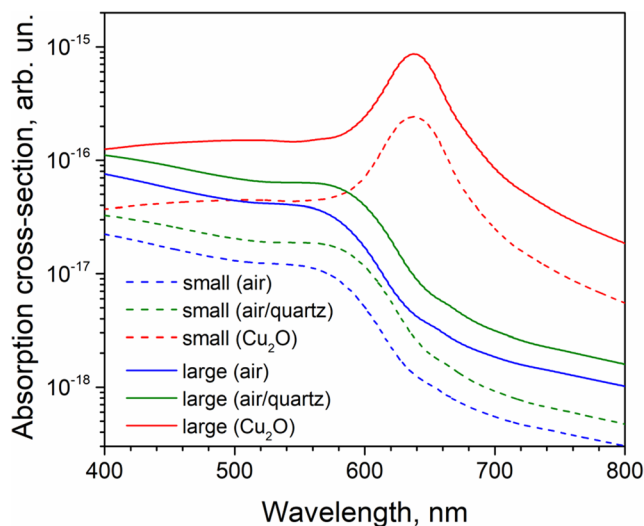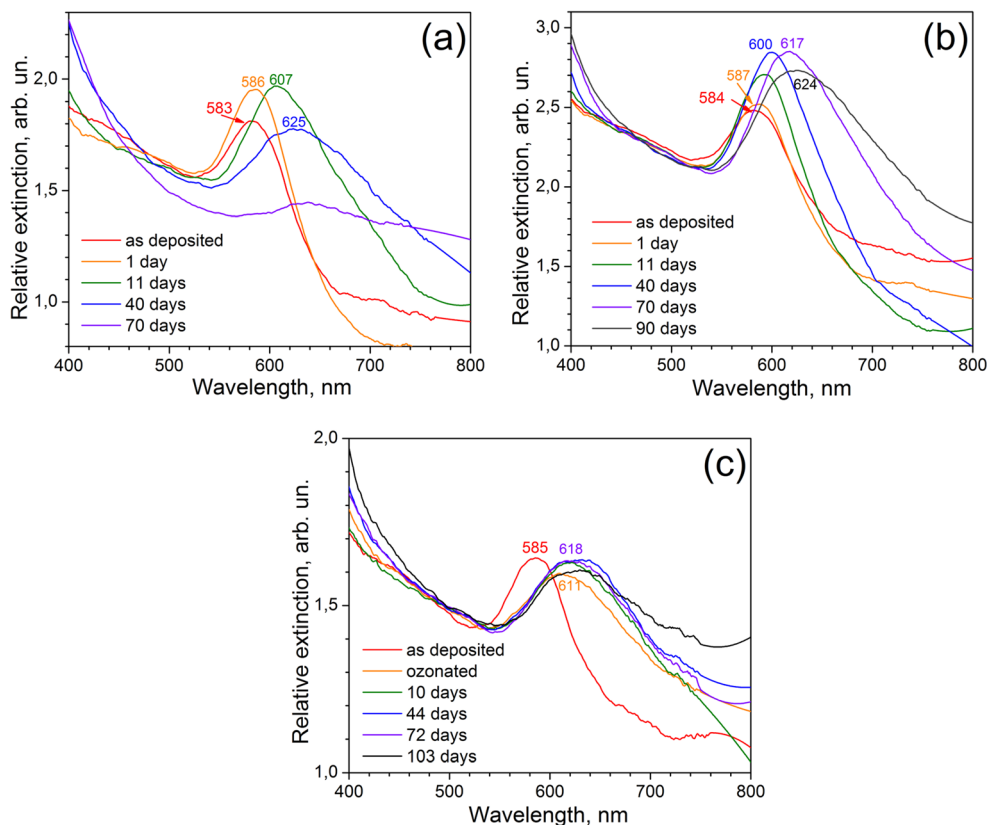
Optical Spectra of Cu NPs

Optical spectra of as-deposited on quartz substrates small NPs presented in Fig. 4 show an LSPR band with a maximum at 584 ± 1 nm. Calculations using the Mie theory predict the plasmon band maximum for spherical Cu NPs in air at a wavelength of approximately 560 nm as can be seen in Fig. 5. Considering an effective dielectric medium approach suggested in [38], where the effective dielectric constant ε_{eff} represents the collective influence of air ($\varepsilon \approx 1.0$) and quartz ($\varepsilon \approx 3.8$) through a weighting factor, allows us to take into account the substrate effect, which leads to a small redshift of the plasmon band and increase of intensity (see Fig. 5), thus, supporting the observed experimental trend.

One day after the deposition, a further small (for 3 nm) redshift of the band maximum and an increase of intensity (see Fig. 4a) are observed. A change of the NP shape from spherical to an oblate (ellipsoid-like) one could lead to this evolution. The same phenomenon was earlier observed for the silver NPs and the corresponding spectral shift was proved by the modelling [29]. Driving force for the oblation is a large difference in surface tension of copper (between ca. 1400 and 1700 mJ/m^2) and quartz (between ca. 57 and 127 mJ/m^2) [39, 40]. The particle tends to minimize the interfacial tension by an increase of the contact area, i.e., flattening from a sphere to an ellipsoid.

Fig. 5 Simulated absorption cross-section vs. wavelength for small (dashed line) and large (solid line) spherical Cu NPs in air ($\varepsilon_{\text{eff}} = 1$), supported on quartz ($\varepsilon_{\text{eff}} = 1.4$), and surrounded by Cu$_2$O ($\varepsilon_{\text{eff}} = 6$)

Growth of an oxide (with high ε) could also lead to the redshift. However, we consider this reason to be less probable because the shift is also observed for the sample stored under nitrogen atmosphere (compare Fig. 4a and b), where the possibility of oxidation during the first day after the deposition is negligible.

Fig. 4 Time evolution of LSPR band for small Cu NPs **a** kept in ambient air, **b** kept in a nitrogen atmosphere, and **c** ozonated and kept in ambient air. Numbers in the panels indicate wavelengths of the band maxima

With time, the plasmon band experiences gradual redshift and an increase of intensity (see Fig. 4a and b). Both the redshift and intensity exhibit a significant change on a long time scale. The most probable scenario is gradual oxidation of the particles leading to an increase of the oxide fraction at the expense of the metallic phase. Thus, the effective medium gradually changes from air/quarts to copper oxide, causing the resonance evolution. The same tendency, although weaker, is observed for the sample kept in N_2 because it was taken into an ambient atmosphere for the optical measurements (see the "Experimental" section for details). The modelling presented in Fig. 5 predicts both a significant redshift and an intensity increase in the case of a copper oxide medium surrounding copper NPs, hence, supporting the proposed scenario. Finally, the plasmon band intensity decreases to almost zero after 70 days for the sample kept in air (see Fig. 4a), while it is preserved for the one kept in N_2 as can be seen in Fig. 4b. This observation further supports the hypothesis about the gradual oxidation of the metallic phase leading to quenching of the LSPR. In Fig. 4c, one can see the spectra for the sample with small NPs treated with UV-ozone and then kept in ambient atmosphere. The formation of the shell predominantly consisting of Cu(II) oxide, as found by XPS and Auger measurements, is the most probable reason preventing

degradation of the plasmonic properties over time. The intensity and wavelength of the LSPR band have been stable for over 100 days as can be seen in Fig. 4c.

Optical spectra of the large NPs are presented in Fig. 6. Similar to the small particles, one can observe a tiny redshift and intensity increase 1 day after the deposition (see Fig. 6a and b), bringing us to the same conclusion about the particle oblation. With time, the plasmon bands experience a redshift together with an intensity increase, thus, showing the same tendency as that observed for the small NPs. Similarly, the redshift is smaller for the sample kept in N_2 atmosphere. The difference in the evolution of the current spectra compared with those of small particles comes at a longer time scale. The plasmon band intensity of the small NPs kept in air started decreasing after approximately 30 days and it became vanishingly small after 70 days (see Fig. 4a), while the LSPR band of the large NPs preserves its intensity up to 3 months; with a slight gradual redshift (Fig. 6a). Since the oxidation occurs at the expense of metallic copper, the larger NPs preserve the metallic phase and, thus, the plasmonic properties for a longer time. The ozonated large NPs are found to have stable plasmonic properties for over 100 days (see Fig. 6c). We only observe a slight redshift, which might be attributed to the slowly increasing thickness of the oxide shell. Thus, one can

Fig. 6 Time evolution of LSPR band for large Cu NPs **a** kept in ambient air, **b** kept in a nitrogen atmosphere, and **c** ozonated and kept in ambient air. Numbers in the panels indicate wavelengths of the band maxima
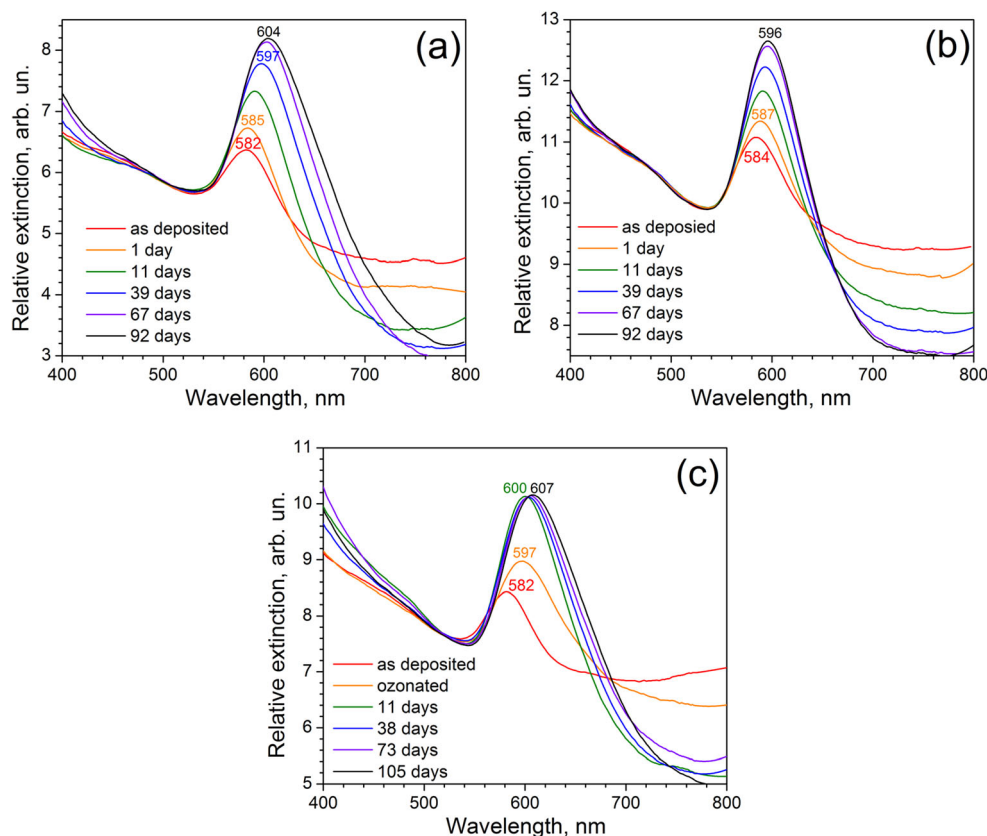
conclude that the UV-ozone treatment is a very efficient (also simple) method to protect the plasmonic properties of Cu NPs against degradation.

The overall impressive stability of the LSPR should be attributed to a monocrystalline structure of the copper NPs produced in magnetron-based aggregation sources, as described in the "Introduction" section. This quality was emphasized for the Ag NPs elsewhere [29], and it is proven for the Cu NPs in the current study. An evidence for higher chemical inertness of Cu NPs produced by magnetron sputtering compared with bulk Cu was also emphasized elsewhere [41], thus, strengthening our conclusion. It is worth mentioning that the suggested UV-ozone treatment is a simpler and cheaper approach compared with many other ways utilizing protective coatings or restoring the metallicity in order to preserve the plasmonic properties of NPs [14, 22, 42 and references therein].

Conclusion

Supported copper NPs produced by the magnetron sputtering gas aggregation method show a strong and narrow LSPR band. On a time scale of 2–3 weeks after the deposition, the band intensity increases and its maximum becomes red-shifted under ambient atmospheric conditions due to the gradual oxidation with the predominant formation of Cu(I) oxide. The oxidation proceeds at the expense of the metallic phase, and at some point in time, the LSPR starts quenching. This process occurs faster for the small NPs, while the large particles demonstrate an extraordinary long (over 90 days) stability of the plasmon band intensity with a slight redshift. This stability is assigned to a high chemical inertness of the NPs due to the perfectness of the crystalline structure formed during the gas aggregation process.

It is found that an UV-ozone treatment of the deposited Cu NPs causes formation of a shell with the domination of Cu(II) oxide. It is supposed that this shell protects the NPs against following oxidation-related degradation of the plasmonic properties leading to the resonance stability on the time scale of > 100 days even for small particles, which without the UV-ozone treatment show the plasmon properties quenching after approximately 60–70 days. Thus, a UV-ozone treatment can be recommended as a simple and effective method for preserving the plasmonic properties of Cu NPs to be used in non-linear optics or sensing applications. Matrixes of Cu NPs can be utilized in surface-enhanced Raman spectroscopy (SERS) of biological objects, where an analyte is often deposited in a liquid phase and chemical stability of NPs is of importance for reliable measurements. Also, spectral position of the plasmon band (580–600 nm) is close to that of the second harmonic of Nd:YAG laser (532 nm), which is one of the standard light sources used in spectroscopy.

References

1. Kreibig U, Vollmer M (1997) Optics of nanosized metals. In: Hummel RE, Wissmann P (eds) Handbook of optical properties, vol 2. CRC Press, Boca Raton, p 145
2. Quinten M (2011) Optical properties of nanoparticle systems. Wiley-VCH, Weinheim
3. Atwater HA, Polman A (2010) Plasmonics for improved photovoltaic devices. Nature Mater. 9:205–213
4. Schuller JA, Barnard ES, Cai W, Jun YC, White JS, Brongersma ML (2010) Plasmonics for extreme light concentration and manipulation. Nature Mater 9:193–204
5. Bharadwaj P, Deutsch B, Novotny L (2009) Optical antennas. Adv Opt Photon 1:438
6. Mosquera J, Zhao Y, Jang H-J, Xie N, Xu C, Kotov NA, Liz-Marzán LM (2019) Plasmonic nanoparticles with supramolecular recognition. Adv Funct Mater 30:1902082
7. Novikov SM, Popok VN, Fiutowski J, Arsenin AV, Volkov VS (2020) Plasmonic properties of nanostructured graphene with silver nanoparticles. J Phys Conf Ser 1461:012119
8. Petryayeva E, Krull UJ (2011) Localized surface plasmon resonance: nanostructures bioassays and biosensing - a review. Anal Chim Acta 706:8–24
9. Langer J, Novikov SM, Liz-Marzán LM (2015) Sensing using plasmonic nanostructures and nanoparticles. Nanotechnol. 26: 322001
10. Rycenga M, Cobley CM, Zeng J, Li W, Moran CH, Zhang Q, Qin D, Xia Y (2011) Controlling the synthesis and assembly of silver nanostructures for plasmonic applications. Chem Rev 111:3669–3712
11. Zhang X, Hicks EM, Zhao J, Schatz GC, Van Duyne RP (2005) Electrochemical tuning of silver nanoparticles fabricated by nanosphere lithography. Nano Lett 5:1503–1507
12. Cao W, Elsayed-Ali HE (2009) Stability of Ag nanoparticles fabricated by electron beam lithography. Mater Lett 63:2263–2266
13. Scuderi M, Esposito M, Todisco F, Simeone D, Tarantini I, De Marco L, De Giorgi M, Nicotra G, Carbone L, Sanvitto D et al (2016) Nanoscale study of the tarnishing process in electron beam lithography-fabricated silver nanoparticles for plasmonic applications. J Phys Chem C 120:24314–24323
14. Chan GH, Zhao J, Hicks EM, Schatz GC, Van Duyne RP (2007) Plasmonic properties of copper nanoparticles fabricated by nanosphere lithography. Nano Lett 7:1947–1952
15. Fedyanin DY, Yakubovsky DI, Kirtaev RV, Volkov VS (2016) Ultralow-loss CMOS copper plasmonic waveguides. Nano Lett 16:362–366
16. Stebunov YV, Yakubovsky DI, Fedyanin DY, Arsenin AV, Volkov VS (2018) Superior sensitivity of copper-based plasmonic biosensors. Langmuir 34:4681–4687
17. Kim JH, Ehrman SH, Germer TA (2004) Influence of particle oxide coating on light scattering by submicron metal particles on silicon wafers. Appl Phys Lett 84:1278–1280
18. LaGrow AP, Ward MR, Lloyd DC, Gai PL, Boyes ED (2017) Visualizing the Cu/Cu$_2$O interface transition in nanoparticles with environmental scanning transmission electron microscopy. J Am Chem Soc 139:179–185

19. Stepanov AL, Popok VN, Hole DE, Khaibullin IB (2002) Ion synthesis and laser annealing of Cu nanoparticles in Al$_2$O$_3$. Appl Phys A Mater Sci Process 74:441–446

20. Popok VN, Nuzhdin VI, Valeev VF, Stepanov AL (2015) Copper nanoparticles synthesized in polymers by ion implantation: surface morphology and optical properties of the nanocomposites. J Mater Res 30:86–92

21. Jimenez JA (2019) Thermal effects on the surface plasmon resonance of Cu nanoparticles in phosphate glass: impact on Cu$^+$ luminescence. Nanoscale Adv 1:1826–1832

22. Kim I, Kim Y, Woo K, Ryu E-H, Yon K-Y, Cao G, Moon J (2013) Synthesis of oxidation-resistant core–shell copper nanoparticles. RSC Adv 3:15169

23. Jardón-Maximino N, Pérez-Alvarez M, Sierra-Ávila R, Ávila-Orta CA, Jiménez-Regalado E, Bello AM, González-Morones P, Cadenas-Pliego G (2018) Oxidation of copper nanoparticles protected with different coatings and stored under ambient conditions. J Nanomater 2018: 9512768

24. Popok VN, Barke I, Campbell EEB, Meiwes-Broer K-H (2011) Cluster-surface interaction: from soft landing to implantation. Surf Sci Rep 66:347–377

25. Huttel Y (ed) (2017) Gas-phase synthesis of nanoparticles. Weinheim, Wiley-WCH

26. Barmparis GD, Lodziana Z, Lopez N, Remediakis IN (2015) Nanoparticle shapes by using Wulff constructions and first-principles calculations. Beilstein J Nanotechnol 6:361–368

27. Martin TP (1996) Shells of atoms. Phys Rep 273:199–241

28. Barke I, Hartmann H, Rupp D, Fluckiger L, Sauppe M, Adolph M, Schorb S, Bostedt C, Treusch R, Peltz C et al (2015) The 3D-architecture of individual free silver nanoparticles captured by X-ray scattering. Nat Commun 6:6187

29. Novikov SM, Popok VN, Evlyukhin AB, Hanif M, Morgen P, Fiutowski J, Beermann J, Rubahn H-G, Bozhevolnyi SI (2017) Highly-stable monocrystalline silver clusters for plasmonic applications. Langmuir 33:6062–6070

30. Popok VN, Hanif M, Ceynowa FA, Fojan P (2017) Immersion of low-energy deposited metal clusters into poly(methyl methacrylate). Nucl Instrum Meth Phys Res B 409:91–95

31. Popok VN, Gurevich L (2019) Charge states of size-selected silver nanoparticles produced by magnetron sputtering. J Nanopart Res 21:171

32. Hartmann H, Popok VN, Barke I, von Oeynhausen V, Meiwes-Broer K-H (2012) Design and capabilities of an experimental setup based on magnetron sputtering for formation and deposition of size-selected metal clusters on ultra-clean surfaces. Rev Sci Instrum 83: 073304

33. Johnson PB, Christy RW (1972) Optical constants of the noble metals. Phys Rev B 6:4370–4379

34. Liu X, Geng B, Du Q, Ma J, Liu X (2007) Temperature-controlled self-assembled synthesis of CuO, Cu$_2$O and Cu nanoparticles through a single-precursor route. Mater Sci Eng A 448:7–14

35. Bok S, Lim GH, Lim B (2017) UV/ozone treatment for adhesion improvement of copper/epoxy interface. J Ind Eng Chem 46:199–202

36. Poulston S, Parlett PM, Stone P, Bowker M (1996) Surface oxidation and reduction of CuO and Cu$_2$O studied using XPS and XAES. Surf Interface Anal 24:811–820

37. Biesinger MC, Lau LWM, Gerson AR, Smart RSC (2010) Resolving surface chemical states in XPS analysis of first row transition metals oxides and hydroxides: Sc Ti V Cu and Zn. Appl Surf Sci 257:887–898

38. Curry A, Nusz G, Chilkoti A, Wax A (2005) Substrate effect on refractive index dependence of plasmon resonance for individual silver nanoparticles observed using darkfield micro-spectroscopy. Opt Express 13:2668–2677

39. Kumykov VK, Sergeev IN, Sozaev VA, Gedgagova MV (2017) Surface tension of copper in solid phase. Bull Rus Acad Sci: Physics 81:357

40. Janczuk B, Zdziennicka A (1994) A study on the components of surface free energy of quartz from contact angle measurements. J Mater Sci 29:3559–3564

41. Martínez L, Lauwaet K, Santoro G, Sobrado JM, Peláez RJ, Herrero VJ, Tanarro I, Ellis GJ, Cernicharo J, Joblin C, Huttel Y, Martín-Gago JA (2018) Precisely controlled fabrication, manipulation and in-situ analysis of Cu based nanoparticles. Sci Rep 8:7250

42. Li Y-F, Dong F-X, Chen Y, Zhang X-L, Wang L, Bi Y-G, Tian Z-N, Liu Y-F, Feng J, Sun H-B (2016) As-grown graphene/copper nanoparticles hybrid nanostructures for enhanced intensity and stability of surface plasmon resonance. Sci Rep 6:37190